Minimally Invasive Therapy & Allied Technologies

ISSN: 1364-5706 (Print) 1365-2931 (Online) Journal homepage: http://www.tandfonline.com/loi/imit20

Optimal approach for complete liver tumor ablation using radiofrequency ablation: a simulation study

Sogol Givehchi, Yin How Wong, Chai Hong Yeong & Basri Johan Jeet Abdullah

To cite this article: Sogol Givehchi, Yin How Wong, Chai Hong Yeong & Basri Johan Jeet Abdullah (2017): Optimal approach for complete liver tumor ablation using radiofrequency ablation: a simulation study, Minimally Invasive Therapy & Allied Technologies, DOI: 10.1080/13645706.2017.1330757

To link to this article: http://dx.doi.org/10.1080/13645706.2017.1330757

MINIMALLY INVASIVE THERAPY & ALLIED TECHNOLOGIES, 2017
https://doi.org/10.1080/13645706.2017.1330757

Taylor & Francis
Taylor & Francis Group

ORIGINAL ARTICLE

Optimal approach for complete liver tumor ablation using radiofrequency ablation: a simulation study

Sogol Givehchi[a], Yin How Wong[a], Chai Hong Yeong[a,b] and Basri Johan Jeet Abdullah[a,b]

[a]Department of Biomedical Imaging, Faculty of Medicine, University of Malaya, Kuala Lumpur, Malaysia; [b]University of Malaya Research Imaging Center, Faculty of Medicine, University of Malaya, Kuala Lumour, Malaysia

ABSTRACT

Purpose: To investigate the effect of radiofrequency ablation (RFA) electrode trajectory on complete tumor ablation using computational simulation.

Material and methods: The RFA of a spherical tumor of 2.0 cm diameter along with 0.5 cm clinical safety margin was simulated using Finite Element Analysis software. A total of 86 points inside one-eighth of the tumor volume along the axial, sagittal and coronal planes were selected as the target sites for electrode-tip placement. The angle of the electrode insertion in both craniocaudal and orbital planes ranged from −90° to +90° with 30° increment. The RFA electrode was simulated to pass through the target site at different angles in combination of both craniocaudal and orbital planes before being advanced to the edge of the tumor.

Results: Complete tumor ablation was observed whenever the electrode-tip penetrated through the epicenter of the tumor regardless of the angles of electrode insertion in both craniocaudal and orbital planes. Complete tumor ablation can also be achieved by placing the electrode-tip at several optimal sites and angles.

Conclusions: Identification of the tumor epicenter on the central slice of the axial images is essential to enhance the success rate of complete tumor ablation during RFA procedures.

ARTICLE HISTORY
Received 26 August 2016
Accepted 24 April 2017

KEYWORDS
Liver tumor; radiofrequency ablation; tumor targeting; electrode trajectory; finite element analysis

Introduction

Liver cancer is the sixth most common cancer worldwide with 782,000 new cases diagnosed in 2012 (1). It is the second leading cause of cancer death, which was responsible for nearly 746,000 deaths globally in 2012 (2). Hepatocellular carcinoma (HCC) is the major histological subtype of primary liver malignancies and accounted for 70–85% of the total liver cancer burden (3). The occurrence of HCC is highly associated with several underlying risk factors such as cirrhosis, type B and C chronic viral hepatitis, alcohol intake as well as aflatoxin exposure (4). Various treatment strategies including surgical resection, systemic therapy, intra-arterial therapy, percutaneous therapy and liver transplantation are available to treat HCC (5).

Over the past two decades, radiofrequency ablation (RFA) has been widely used for small primary and metastatic tumors (6). The overall and disease-free survival rates of RFA are found comparable to those observed with surgical resection (7). In addition, RFA has been proven to be more effective than percutaneous ethanol injection for local tumor control and has led to lesser side effects compared to other ablative procedures (8–10). An effective RFA treatment can be accomplished through a complete tumor ablation together with a clinical safety margin of at least 0.5 cm (11,12). The success rate of complete tumor ablation is highly dependent on tumor targeting precision, which is governed by two major factors, i.e., electrode-tip placement and angulation for electrode insertion. Various previous studies have demonstrated the failure of RFA in ablating the tumor completely due to the inability in determining the optimal electrode insertion site and angulation (13,14).

In order to increase the success rate of complete tumor ablation, various attempts have been made to improve tumor targeting precision and RFA electrode trajectory planning (13–20). For instance, preoperative and intraoperative treatment planning software has been developed to provide a 3D view of the patient's segmented anatomy and simulation of the RFA electrode in 3D virtual space (13). In addition, different

CONTACT Chai Hong Yeong chyeong@um.edu.my Department of Biomedical Imaging, Faculty of Medicine, University of Malaya, 50603 Kuala Lumpur, Malaysia

Supplemental data for this article can be accessed here.

protocols and models have been designed to determine the number of RFA required and electrode placement for larger hepatic tumors using single or multiple RFA electrodes (14,16). Several interventional navigation systems which contain pre-operative and intra-operative modules have also been developed and widely used in the treatment of non-resectable liver tumors (15,17–19). The pre-operative module allows the identification of the target volume, tumor segmentation and determination of the surgical plan including center of the tumor, electrode puncture site on the skin and RFA electrode trajectory. Meanwhile, the intra-operative module comprised the tracking system to visualize the position of the electrode into the coordinate of pre-loaded medical images and registration to show the correlation of spatial orientation of the patient in the operating room and the patient's pre-operative images.

Although many efforts have been directed to improve tumor targeting and RFA electrode trajectory, nonetheless, the effects and importance of electrode angulation in the orbital and craniocaudal planes as well as variation in the electrode-tip placement relative to *x*-, *y*- and *z*-axes in the Cartesian coordinate system on the success rate of complete tumor ablation are yet to be evaluated. Hence, this study was carried out to investigate the effects of electrode placement along the *x*-, *y*- and *z*-axes and the electrode insertion angle on complete tumor ablation using a computational simulation model.

Material and methods

Computational simulation model

A computational simulation model (Figure 1(A,B)) was developed to investigate the effect of RFA electrode trajectory inside a tumor on the success rate of complete tumor ablation. The simulation model was developed based on the following assumptions:

- The tumor is a perfect sphere with 1.0 cm radius.
- The clinical safety margin for tumor ablation is 0.5 cm.
- The ablation zone created by a single RFA electrode from the Cool-Tip RFA system (Covidien, Mansfield, MA) is an ellipse with a minor-axis of 3.1 cm and a major-axis of 3.7 cm (21–24).

In order to study the effect of the RFA electrode trajectory on complete tumor ablation, three preliminary steps were performed. First, specified locations within the tumor were selected as electrode passage points. Then, certain degrees of angle in the

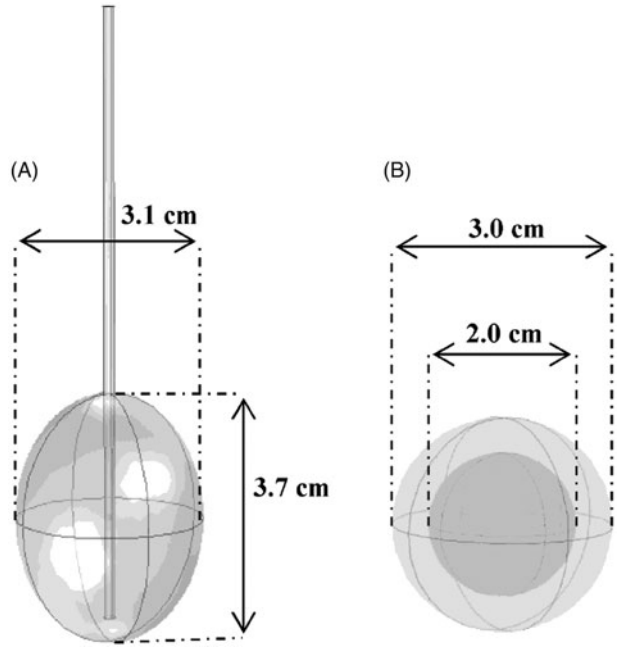

Figure 1. Computational simulation model of (A) RFA electrode and ellipsoidal-shaped ablation and (B) spherical-shaped tumor and its safety margin.

combination of orbital and craniocaudal planes were determined for electrode insertion. Finally, the coordinates of the electrode-tip and center of the ablation in the three-dimensional (3D) Cartesian coordinate system were determined using Matlab (MathWorks Inc., Natick, MA) software. The computational model of tumor ablation using RFA was then simulated using Finite Element Analysis software Comsol Multiphysics 4.2a+ (COMSOL Inc., Palo Alto, CA) to calculate the missed ablated volume of the tumor.

Determination of electrode passage location

The spherically shaped tumor was divided into eight equal parts and one-eighth of the volume was used to sketch the electrode trajectory inside the tumor. The axial, coronal and sagittal planes were employed to segment the selected volume into smaller parts. The parallel axial planes were arranged along the *z*-axis with 0.2 cm distance from each other. In the same way, the parallel coronal and parallel sagittal planes were arranged along the *y*-axis and the *x*-axis, respectively (Figure 2(A)). These different planes intersected each other at 86 points in the 3D space. The location of each intersection point in the Cartesian coordinate system represents the coordinate of the point (with a distance of 0.2 cm to its neighbor points) where the RFA electrode was supposed to penetrate through it before being pushed toward the distal edge of the tumor.

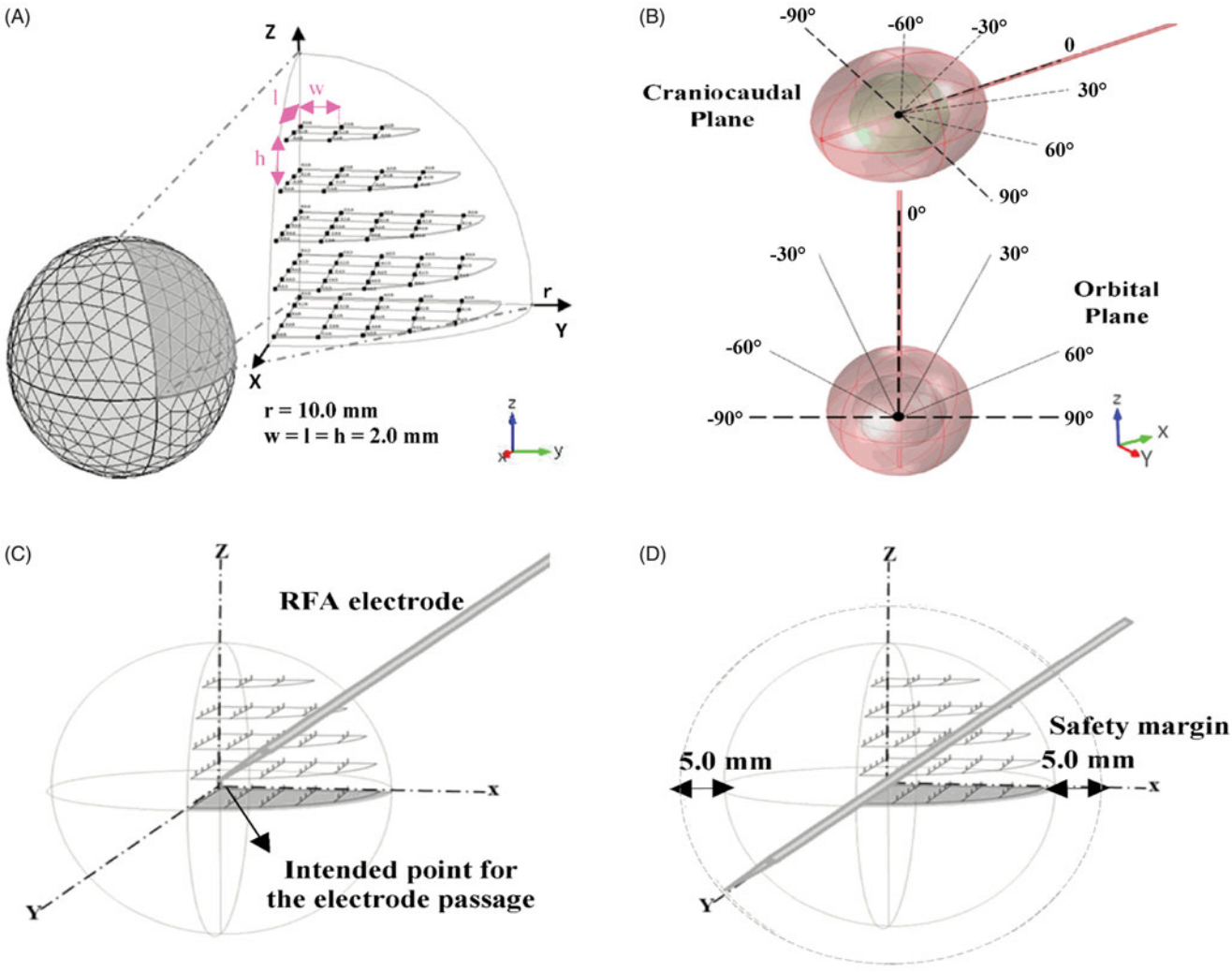

Figure 2. (A) One-eighth of the tumor volume was segmented into different electrode insertion points of 0.2 cm interval along the axial, sagittal and coronal planes, resulting in a total of 86 electrode-tip passage points within one-eighth of the tumor. (B) The RFA electrode was inserted into the tumor at various angles (−90° to +90° with a 30° increment) in the craniocaudal and orbital planes. (C) The RFA electrode was inserted into the intended point. (D) The RFA electrode was pushed toward the posterior end of the tumor to create a 0.5 cm safety margin.

Determination of electrode insertion angulation

The electrode-tip should be inserted at the intended points at different angles in the craniocaudal and orbital planes. The spherical coordinate was used for the better display of azimuthal (ϕ) and polar (θ) angles in which they were varied in the craniocaudal plane (i.e., in the xy plane from the x-axis) and orbital plane (i.e., from the positive z-axis), respectively. The angles in the craniocaudal plane were varied at −90°, −60°, −30°, 0°, 90°, 60° and 30°, while the angle of the electrode insertion was varied in the orbital plane at −90°, −60°, −30°, 0°, 30°, 60° and 90° for each mentioned craniocaudal plane angle (Figure 2(B)). Theoretically, the electrode should be inserted at a particular angle into the specified point of the tumor and pushed toward the posterior end of the tumor to create a clinical margin of 0.5 cm (Figure 2(C,D)).

Determination of the position of electrode-tip and center of ablation

The exact position of the electrode-tip and the center of ablation in the 3D space were calculated using Matlab software. In order to localize the position of the electrode-tip, the intersection point between the tumor together with its safety margin (a sphere) and the electrode (a line) was calculated. The coordinate of the point on a line (location of the electrode passage) and its unit vector (angle of the electrode insertion) were used to calculate the line equation. The equation of the line that passed through the point

(x_0, y_0, z_0) and parallel to non-zero vector (p, q, g) is given as:

$$(x, y, z) = (x_0, y_0, z_0) + (p, q, g)t \quad (1)$$

The coordinate of (x_0, y_0, z_0) was calculated in the prior section for 86 different points within the tumor in the Cartesian coordinate system. The Cartesian coordinate (p, q, g) was determined from the spherical coordinate of r, θ and ϕ using Equations (2)–(4):

$$p = r\cos\phi\ \sin\theta \quad (2)$$

$$q = r\sin\phi\ \sin\theta \quad (3)$$

$$g = r\ \cos\theta \quad (4)$$

where r as a unit vector with a magnitude of 1, ϕ and θ are azimuthal and planar angles of the electrode insertion, respectively.

The equation for the sphere is as follow:

$$(x-a)^2 + (y-b)^2 + (z-c)^2 = R^2 \quad (5)$$

where (x, y, z) is the coordinate of a point on the sphere; (a, b, c) = (0, 0, 0) is the coordinate of the center of the tumor and R (1.5 cm) is the radius of the sphere (i.e., 1.0 cm tumor radius plus 0.5 cm clinical margin). Finally, the parametric equation of a line was substituted into the sphere equation to calculate the exact location of the electrode tip on the safety margin of the tumor (Figure 3(A)).

In order to find out the position of the ablation in 3D space, the coordinate of the center point (i.e., intersection point between minor-axis and major-axis of the ablation) was calculated (Figure 3(B)). Since the direction of the electrode and ablation were the same

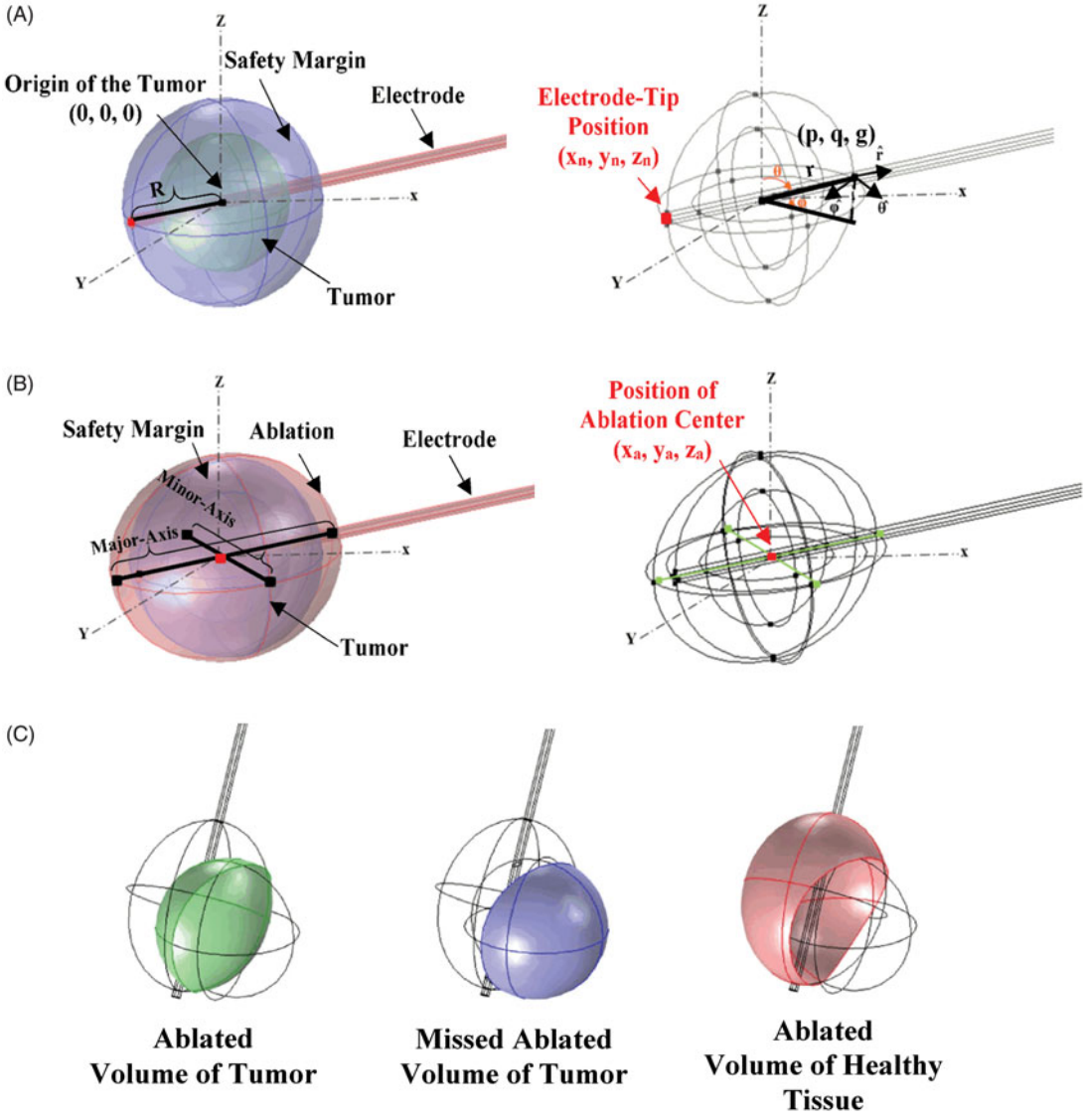

Figure 3. (A) The position of the electrode-tip in the Cartesian coordinate system and direction of the electrode in the spherical coordinate. (B) The position of center of the ablation in the Cartesian coordinate system. (C) Diagrams showing the ablated volume of the tumor, the missed ablated volume of the tumor and the ablated volume of the healthy tissue.

and the center of the ablation was located with a specific distance from the electrode-tip position, the unit vector of the electrode and location of the electrode-tip were used to calculate the position of the ablation center point (Equation (6)):

$$(x_a,\ y_a, z_a) = (x_n,\ y_n, z_n) + (p,\ q, g) \cdot \sqrt{\frac{R^2}{(p^2+q^2+g^2)}} \quad (6)$$

where (x_a, y_a, z_a) is the center point coordinate of the ablation and (x_n, y_n, z_n) is the coordinate of the electrode-tip.

Measurement of missed ablated volume of the tumor

The COMSOL Multiphysics software (COMSOL, Burlington, MA) was used to calculate the ablated volume of the tumor, which was defined as the common volume between tumor and ellipsoidal-shaped ablation, for different angles at each target point. The ablated volume of the tumor was marked manually and measured using different measurement options available from the software. The volume of the tumor was calculated using Equation (7):

$$v_{\text{sphere}} = \frac{4}{3}\pi R^3 \quad (7)$$

The missed ablated volume (cm^3) was calculated by subtracting the ablated volume from the volume of the tumor using the following equation (Figure 3(C)):

$$v_{\text{missed}} = v_{\text{tumor}} - v_{\text{ablated}} \quad (8)$$

Measurement of ablated volume of the healthy tissue

In order to calculate the volume of the damaged tissue at the surrounding of the tumor, the volume of ellipsoidal-shaped ablation was subtracted from the common volume between the tumor and ablation (ablated volume) (Figure 3(C)) where the volume of the ellipsoidal-shaped ablation was calculated using Equation (9):

$$v_{\text{oblation}} = \frac{4}{3}\ abc \quad (9)$$

where b and c are minor radiuses and a is major radius of ellipse.

The volume of the damaged tissue at the surrounding of the tumor was then calculated using Equation (10):

$$v_{\text{damaged}} = v_{\text{ablation}} - v_{\text{ablated}} \quad (10)$$

Results

Electrode placement was simulated for a total of 86 points distributed from the center of the tumor towards its edge along the x-, y- and z-axes (Figure 2(A)). The angle for electrode insertion at each target point was varied from $-90°$ to $+90°$ with a $30°$ increment in the combination of both craniocaudal and orbital planes (Figure 2(B)). The ablated volume, missed ablated volume and ablated volume of healthy tissue for all 4214 simulations were calculated using geometric calculation as described above and are listed in Supplementary Table 1. The electrode insertion points and angles, which resulted in zero missed ablated volume and smallest possible healthy tissue damage, were considered as the optimal target sites and angles for electrode insertion. The location of the optimal target sites and their associated angles are marked in red color in Supplementary Table 1.

Effect of electrode-tip placement on complete tumor ablation

In order to investigate the effect of electrode-tip passageway within the tumor on the success rate of complete tumor ablation, the electrode insertion angulation was fixed at a constant angle (i.e., $90°$, $60°$, $30°$, $0°$, $-30°$, $-60°$ and $-90°$) while changing the electrode-tip placement location. Figure 4 shows the 3D graph designed to display the missed ablated volumes of the tumor when the electrode passed through different passage points located in the tumor at a particular insertion angle (e.g., $\phi = 0°$ and $\theta = 90°$, $60°$, $30°$, $0°$, $-30°$, $-60°$ and $-90°$). Each graph contains 86 cubes where their positions corresponded to the locations of the electrode passage points and the widths indicated the missed ablated volume of the tumor. The degree of missed ablated volume can also be seen from the color spectrum (from white to dark red) where the darker color indicated the greater missed ablated volume. Generally, the lighter color cubes (lower missed ablated volume) were concentrated around the center of the tumor (Figure 4) with an exception for the graph obtained at $\theta = 60°$ where the lighter cubes were widely distributed along the x-, y- and z-axes (Figure 4(C)). In addition, the variation in electrode passage point along x- and z-axes for the graphs obtained at $\theta = \pm 90°$ and $\theta = 0°$ did not affect the success rate of complete tumor ablation (Figure 4(A,B)).

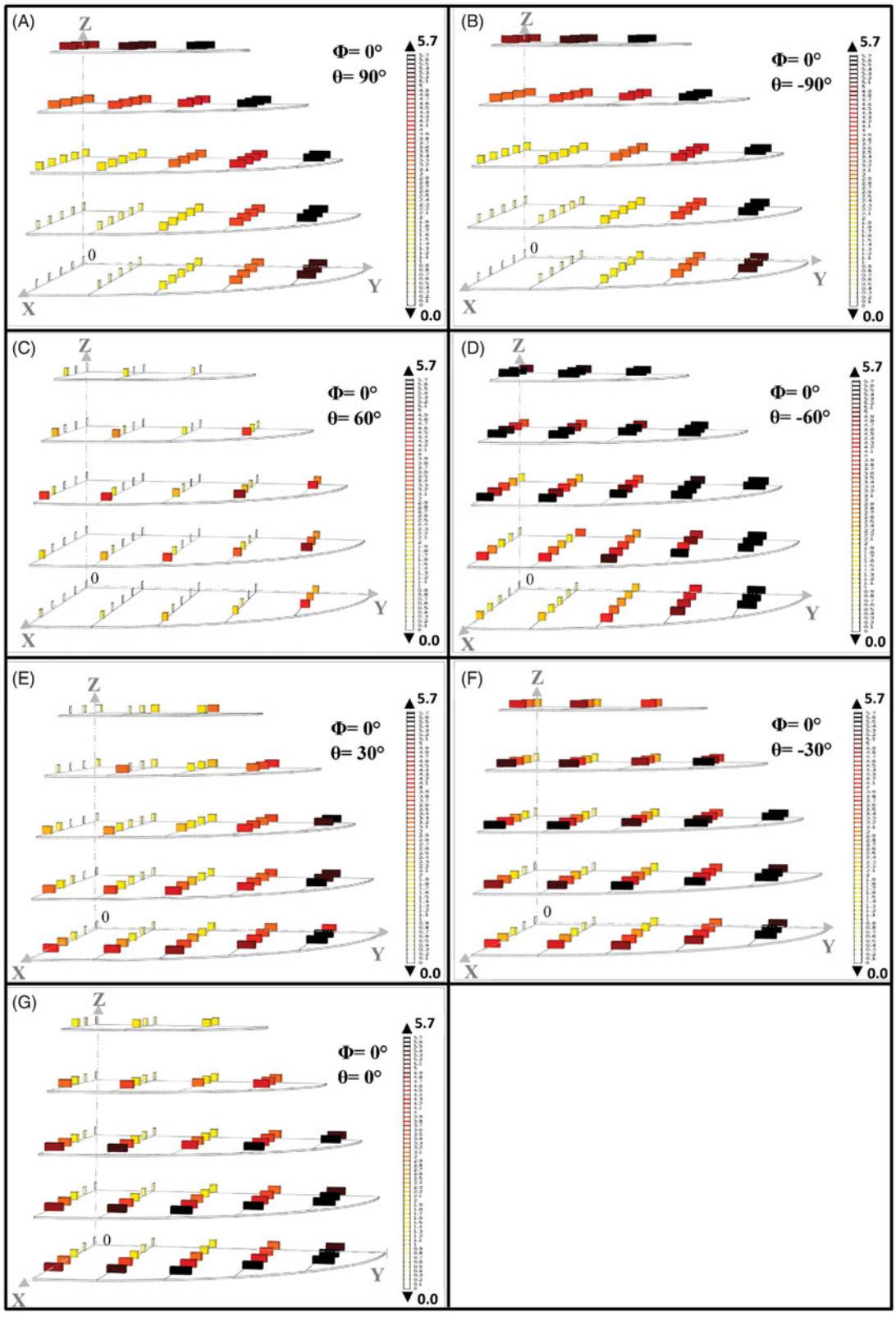

Figure 4. Distribution of the missed ablated volume of the tumor along *x*-, *y*- and *z*-axes in the 3D graph at electrode insertion angle of (A) $\Phi = 0^\circ$ and $\theta = 90^\circ$; (B) $\Phi = 0^\circ$ and $\theta = -90^\circ$; (C) $\Phi = 0^\circ$ and $\theta = 60^\circ$; (D) $\Phi = 0^\circ$ and $\theta = -60^\circ$; (E) $\Phi = 0^\circ$ and $\theta = 30^\circ$; (F) $\Phi = 0^\circ$ and $\theta = -30^\circ$; (G) $\Phi = 0^\circ$ and $\theta = 0^\circ$. The width of the cube represented the missed ablated volume of the tumor in cm^3, whereas the color spectrum reflected the missed ablated volume with the dark red showing the most missed ablated volume. The color spectrum started from 0 to 5.7 cm^3 with 0.1 cm^3 interval.

Table 1. The numbers of the ideal point (***n***) and the location in the Cartesian coordinate system for electrode insertion at different orbital plane angles, while the craniocaudal plane angle was set at 0°.

Orbital plane angle	Number ofideal point	Coordinate of ideal point		
		x	*y*	*z*
90°	5	0	0	0
		0.2	0	0
		0.4	0	0
		0.6	0	0
		0.8	0	0
60°	4	0	0	0
		0.4	0	0.2
		0.6	0	0.4
		0.8	0	0.4
30°	5	0	0	0
		0.2	0	0.4
		0.4	0	0.4
		0.4	0	0.6
		0.4	0	0.8
0°	5	0	0	0
		0	0	0.2
		0	0	0.4
		0	0	0.6
		0	0	0.8
30°	1	0	0	0
60°	1	0	0	0
90°	5	0	0	0
		0.2	0	0
		0.4	0	0
		0.6	0	0
		0.8	0	0

Effect of electrode insertion angle on complete tumor ablation

The number of the ideal point (***n***) at each particular angle where the missed ablated volume of the tumor is zero was used to determine the best angle for electrode insertion. Table 1 shows the location of the ideal points and their ***n*** value at electrode-tip insertion angles of (ϕ, θ) = (0°, 90°), (0°, 60°), (0°, 30°), (0°, 0°), (0°, −30°), (0°, −60°) and (0°, −90°). The highest ***n*** value (***n*** = 5) was observed for the orbital plane angles of +90°, +30°, 0° and −90° followed by +60° (***n*** = 4) when the craniocaudal plane angle was set at 0°. The orbital plane angles of 30° and 60° obtained the lowest ***n*** value of 1 (Table 1). The numbers of the ideal points for the electrode insertion at different angles in both the craniocaudal and orbital planes are given in Table 2. The locations of these points in the Cartesian coordinate system are listed in Supplementary Table 2. As can be seen from the table, the ***n*** value of 5 was obtained for different craniocaudal plane angles at 90°, 60°, 30°, 0°, −30°, −60° and −90° when the orbital plane angle was set at 0°. The combination of different craniocaudal and orbital plane angles (ϕ, θ) at (90°, 90°), (0°, 90°), (−90°, 90°), (0°, 30°), (90°, −90°), (−90°, 90°), (0°, −90°) and (−90°, −90°) also obtained ***n*** value of 5 (Table 2).

Table 2. The number of the ideal point (***n***) for electrode insertion at different angles in the craniocaudal and orbital planes.

Orbital plane angle	Craniocaudal plane angles						
	90°	60°	30°	0°	−30°	−60°	−90°
90°	5	4	4	5	1	1	5
60°	4	2	2	4	1	1	1
30°	4	2	2	5	1	1	1
0°	5	5	5	5	5	5	5
−30°	1	1	1	1	1	1	4
−60°	1	1	1	1	1	1	4
−90°	5	4	4	5	1	1	5

Discussion

Generally, electrode insertion points which are nearer to the center of the tumor along the *x*-, *y*- or *z*-axes have a higher probability to achieve complete tumor ablation with a lower degree of healthy tissue damage. The highest incident of complete tumor ablation was found concentrated at the center of the tumor. In other words, the incident of tumor missed ablation increased when the location of the electrode-tip placement is further away from the center of the tumor. Based on the ***n*** value obtained at different angles, the best orbital plane angles for RFA electrode insertion to achieve complete tumor ablation are +90°, +30°, 0° and −90°. The second rank orbital plane angle for electrode insertion is at +60° while the insertion angles of −30° and −60° have the lowest probability to achieve complete tumor ablation. On the contrary, when the orbital plane angle is set at 0°, complete tumor ablation was observed for all the craniocaudal angles studied. Furthermore, the combination of the angles +90°, +30°, 0° and −90° in both orbital and craniocaudal planes also resulted in complete tumor ablation. In view of the above, the insertion angles of +90°, +30°, 0° and −90° in both orbital and craniocaudal planes are the optimal angles to achieve complete tumor ablation.

Tumor targeting precision is important to ensure a complete tumor ablation using RFA (20). Accurate electrode placement is not only critical to warrant a technical success of RFA, but also vital to prevent local tumor recurrence by ablating the clinical safety margin of 0.5 cm surrounding the tumor (7,25). Often, imprecise tumor targeting or electrode placement could compromise the safety of the patient who undergoes an RFA procedure. Several major complications such as pleural and gastrointestinal perforations, laceration of vessels with bleeding, thermal collateral damage with bile duct stenosis, biloma, gastrointestinal inflammation and subsequent perforation are known to occur due to imprecise tumor targeting (26–28). Some of these complications such as

perforation of the gastrointestinal wall have been proven to be fatal (26,27).

Conventionally, the center of the tumor was preoperatively defined by the radiologists as the electrode-tip placement to achieve complete tumor ablation (25). However, the electrode trajectory (insertion angle and electrode-tip placement) would be subjected to change if the critical organs or bones obstructed the electrode passageway. Our results indicated that complete tumor ablation can be achieved by passing the electrode through the center of the tumor, regardless of the angle of electrode insertion. Hence, if the electrode-tip was placed at the epicenter of the tumor, the electrode insertion angle in combination of craniocaudal and orbital planes can be altered in order to change the electrode trajectory before advancing it to the edge of the tumor margin. Furthermore, the electrode trajectory can also be altered by changing the location of the electrode-tip placement to achieve complete tumor ablation. The numbers and coordinates of optimal target sites where a complete tumor ablation can be achieved at different electrode insertion angles are shown in Table 2 and Supplementary Table 2, respectively. The electrode insertion angle of 0° in both craniocaudal and orbital planes provided the maximum number of optimal target sites for complete ablation.

Despite dependence on the electrode trajectory, complete tumor ablation also depends on the ablation time where longer ablation time is needed to achieve a larger ablation size. For instance, the ablation size created by a single Cool-Tip RF electrode for the duration of 6 min is 2.3 cm in diameter but is increased to 3.1 cm when the ablation time increases to 12 min. In clinical practice, the ablation time is determined based on the size of the tumor (with defined clinical margins) and in accordance with the protocol recommended by the respective manufacturer.

Several limitations were identified in our study. First, the 3D model used in this study was developed on the basis of a theoretic spherical-shaped tumor (2.0 cm diameter) with 0.5 cm clinical margin and a single ellipsoidal-shaped ablation (minor-diameter 3.1 cm and major-diameter 3.7 cm). In reality, the ablation zone created by the Cool-Tip RFA depends on tissue vascularization, tissue properties, temperature and impedance of the tissue. However, our study assumed that the ablation created by the single Cool-Tip electrode is a single ellipsoidal-shaped ablation. In order to obtain a more comprehensive analysis, a general 3D model with different tumor sizes and ablation zones for single and multiple ablations should be developed. Second, the number of electrode-tip placements in this study was limited to 86 target sites selected within one-eighth of the tumor volume. Lastly, a limited range of angulation (i.e., from −90° to +90° with 30° increment in both craniocaudal and orbital planes) was simulated for electrode insertion. A more accurate study on the effects of electrode-tip placement and angle of electrode insertion on the probability of complete tumor ablation can be achieved by increasing the number of target sites and extending the range of insertion angles. Although this preliminary study included the above limitations, nevertheless, it provided some insight on the improvement of tumor targeting accuracy in order to achieve a higher success rate of complete tumor ablation by RFA.

Conclusions

Tumor targeting and electrode angulation are two important factors affecting the success rate of complete tumor ablation. The probability of complete tumor ablation is greatly enhanced by identifying the optimal target site and angle for electrode insertion. Our results indicated that complete tumor ablation can be constantly achieved by passing the electrode through the epicenter of the tumor before advancing it to the edge of the tumor margin regardless of the angle of electrode insertion. Moreover, complete tumor ablation can also be achieved if the electrode is inserted at a specified angle within the optimal target site.

Acknowledgements

This work was financially supported by Science Fund [SF011–2014] sanctioned by the Ministry of Science, Technology and Innovation, Malaysia to CHY. Preliminary data of this study have been presented at the World Congress on Medical Physics and Biomedical Engineering at Metro Toronto Convention Centre, Toronto, Canada on 6 November 2015.

Declaration of interest

The authors report no conflicts of interest.

Funding

This work was financially supported by Science Fund [SF011–2014] sanctioned by the Ministry of Science, Technology and Innovation, Malaysia to CHY.

References

1. International World Cancer Research Fund International 2016. Available at: http://www.wcrf.org/int/cancer-facts-figures/worldwide-data [Accessed May 3, 2016].
2. GLOBACAN. Liver Cancer – Estimated Incidence, Mortality and Prevalence Worldwide in 2012. 2012. Available at: http://globocan.iarc.fr/old/FactSheets/cancers/liver-new.asp#INCIDENCE1 [Accessed May 3, 2016].
3. El-Serag HB. Hepatocellular carcinoma. N Engl J Med 2011;365:1118–27.
4. El-Serag HB, Mason AC. Rising incidence of hepatocellular carcinoma in the United States. N Engl J Med 1999;340:745–50.
5. Orsi F. HCC. In: Van Cutsem E, Vogl JT, Orsi F, Sobrero A, editors. Locoregional Tumor Therapy. Berlin, Heidelberg: Springer Berlin Heidelberg; 2015. pp 31–54.
6. Lencioni R, Cioni D, Crocetti L, Franchini C, Pina CD, Lera J, et al. Early-stage hepatocellular carcinoma in patients with cirrhosis: long-term results of percutaneous image-guided radiofrequency ablation. Radiology 2005;234:961–7.
7. Minami Y, Kudo M. Radiofrequency ablation of hepatocellular carcinoma: a literature review. Int J Hepatol 2011;2011:104685.
8. Gillams AR. Radiofrequency ablation in the management of liver tumours. Eur J Surg Oncol 2003;29:9–16.
9. Ikeda M, Okada S, Ueno H, Okusaka T, Kuriyama H. Radiofrequency ablation and percutaneous ethanol injection in patients with small hepatocellular carcinoma: a comparative study. Jpn J Clin Oncol 2001;31:322–6.
10. Livraghi T, Goldberg SN, Lazzaroni S, Meloni F, Solbiati L, Gazelle GS. Small hepatocellular carcinoma: treatment with radio-frequency ablation versus ethanol injection. Radiology 1999;210:655–61.
11. Goldberg SN, Grassi CJ, Cardella JF, Charboneau JW, Dodd GD III, Dupuy DE, et al. Image-guided tumor ablation: standardization of terminology and reporting criteria. J Vasc Interv Radiol 2005;16:765–78.
12. Park MH, Rhim H, Kim YS, Choi D, Lim HK, Lee WJ. Spectrum of CT findings after radiofrequency ablation of hepatic tumors. Radiographics 2008;28:379–92.
13. Butz T, Warfield SK, Tuncali K, Silverman SG, van Sonnenberg E, Jolesz FA, et al. Pre- and intra-operative planning and simulation of percutaneous tumor ablation. In: Delp SL, DiGoia AM, Jaramaz B, editors. Medical Image Computing and Computer-Assisted Intervention – MICCAI 2000: Third International Conference; October 11–14, 2000 Proceedings; Pittsburgh, PA, USA. Berlin, Heidelberg: Springer Berlin Heidelberg; 2000. pp 317–26.
14. Chen M-H, Yang W, Yan K, Zou M-W, Solbiati L, Liu J-B, et al. Large liver tumors: protocol for radiofrequency ablation and its clinical application in 110 patients-mathematic model, overlapping mode, and electrode placement process. Radiology 2004;232:260–71.
15. Bale R, Widmann G. Navigated CT-guided interventions. Minim Invasive Ther Allied Technol 2007;16:196–204.
16. Dodd GD III, Soulen MC, Kane RA, Livraghi T, Lees WR, Yamashita Y, et al. Minimally invasive treatment of malignant hepatic tumors: at the threshold of a major breakthrough. Radiographics 2000;20:9–27.
17. Phee SJ, Yang K. Interventional navigation systems for treatment of unresectable liver tumor. Med Biol Eng Comput 2010;48:103–11.
18. Uddin FJ, Sama A, Jones NS. Three-dimensional computer-aided endoscopic sinus surgery. J Laryngol Otol 2003;117:333–9.
19. Widmann G, Stoffner R, Sieb M, Bale R. Target registration and target positioning errors in computer-assisted neurosurgery: proposal for a standardized reporting of error assessment. Int J Med Robot Comp 2009;5:355–65.
20. Acosta Ruiz V, Lönnemark M, Brekkan E, Dahlman P, Wernroth L, Magnusson A. Predictive factors for complete renal tumor ablation using RFA. Acta Radiol 2015;57:886–93.
21. Ng KK, Lam CM, Poon RT, Shek TW, Yu WC, To JY, et al. Porcine liver: morphologic characteristics and cell viability at experimental radiofrequency ablation with internally cooled electrodes. Radiology 2005;235:478–86.
22. Rathke H, Hamm B, Guttler F, Rathke J, Rump J, Teichgraber U, et al. Comparison of four radiofrequency ablation systems at two target volumes in an *ex vivo* bovine liver model. Diagn Interv Radiol (Ankara, Turkey) 2014;20:251–8.
23. Rubert N, Bharat S, DeWall RJ, Andreano A, Brace C, Jiang J, et al. Electrode displacement strain imaging of thermally-ablated liver tissue in an *in vivo* animal model. Med Phys 2010;37:1075–82.
24. Haemmerich D, Chachati L, Wright AS, Mahvi DM, Lee FT Jr, Webster JG. Hepatic radiofrequency ablation with internally cooled probes: effect of coolant temperature on lesion size. IEEE Trans Biomed Eng 2003;50:493–500.
25. Abdullah BJ, Yeong CH, Goh KL, Yoong BK, Ho GF, Yim CC, et al. Robotic-assisted thermal ablation of liver tumours. Eur Radiol 2015;25:246–57.
26. Choi H, Loyer EM, DuBrow RA, Kaur H, David CL, Huang S, et al. Radio-frequency ablation of liver tumors: assessment of therapeutic response and complications. Radiographics 2001;21:S41–S54.
27. Livraghi T, Solbiati L, Meloni MF, Gazelle GS, Halpern EF, Goldberg SN. Treatment of focal liver tumors with percutaneous radio-frequency ablation: complications encountered in a multicenter study. Radiology 2003;226:441–51.
28. Rhim H, Gerald D, Dodd I, Chintapalli KN, Wood BJ, Dupuy DE, et al. Radiofrequency thermal ablation of abdominal tumors: lessons learned from complications. Radiographics 2004;24:41–52.